C. R. Mecanique 343 (2015) 410–418

Contents lists available at ScienceDirect

Comptes Rendus Mecanique

www.sciencedirect.com

A new method to determine the true projected contact area using nanoindentation testing

Une nouvelle méthode pour déterminer l'aire de contact projetée réelle par nano-indentation

Gaylord Guillonneau [a,b,*], Guillaume Kermouche [c], Jean-Michel Bergheau [d], Jean-Luc Loubet [b]

[a] *EMPA, Swiss Federal Laboratories for Materials Science and Technology, Laboratory for Mechanics of Materials and Nanostructures, Feuerwerkerstrasse 39, 3602 Thun, Switzerland*
[b] *École centrale de Lyon, Laboratoire de tribologie et dynamique des systèmes, UMR 5513 CNRS/ECL/ENISE, 36, avenue Guy-de-Collongue, 69134 Écully, France*
[c] *École des mines de Saint-Étienne, Centre SMS, Laboratoire LGF UMR5307, 158, cours Fauriel, 42023 Saint-Étienne, France*
[d] *Université de Lyon, ENISE, LTDS, UMR 5513 CNRS, 58, rue Jean-Parot, 42023 Saint-Étienne cedex 2, France*

ARTICLE INFO

Article history:
Received 5 February 2015
Accepted 22 June 2015
Available online 15 July 2015

Keywords:
Nanoindentation
Projected contact area
Model
Representative stress
Hardness
Modulus of elasticity

Mots-clés :
Nanoindentation
Aire de contact projetée
Modèle
Contrainte représentative
Dureté
Module d'élasticité

ABSTRACT

A new technique to determine the true projected contact area by nanoindentation is presented. It requires combining two models used normally to determine the representative stress and strain from nanoindentation parameters. Consequently, it does not require any model classically used to calculate the projected contact area. The method requires performing indentation on the same sample with two indenter tips with different geometries (Berkovich tip and a tetrahedral tip with a semi-angle equal to 50°). The method was applied to three samples: glass, PMMA, and 100C6 steel. The projected contact area obtained by this model was accurate in all cases.

RÉSUMÉ

Une nouvelle technique de mesure de l'aire de contact projetée par nano-indentation est présentée. Elle requiert la combinaison de deux modèles habituellement utilisés pour la détermination des contraintes et déformations représentatives à partir des paramètres mesurés en nano-indentation. Les modèles utilisés habituellement pour calculer l'aire de contact projetée ne sont donc pas utilisés. Cette nouvelle méthode nécessite d'effectuer les tests d'indentation sur le même échantillon en utilisant deux indenteurs de géométrie différente (pointe Berkovich et pointe tétraédrale, dont le demi-angle au sommet est de 50°). La méthode a été appliquée sur trois échantillons : verre, PMMA et acier 100C6.

* Corresponding author at: EMPA, Swiss Federal Laboratories for Materials Science and Technology, Laboratory for Mechanics of Materials and Nanostructures, Feuerwerkerstrasse 39, 3602 Thun, Switzerland. Tel.: +41 (0)587656311; fax: +41 (0)587656990.
E-mail address: gaylord.guillonneau@empa.ch (G. Guillonneau).

http://dx.doi.org/10.1016/j.crme.2015.06.004
1631-0721/

L'aire de contact projetée obtenue avec ce modèle a été mesurée de façon précise pour tous les échantillons.

1. Introduction

The instrumented nanoindentation technique is commonly used to probe surface mechanical properties at the nanometer scale. The technique consists in applying a normal load with an indenter tip of known geometry on a sample, and recording the tip displacement. This technique can be used to measure the mechanical properties of bulk materials, thin films samples or structured materials. With only one test, this non-destructive technique can measure the hardness and the reduced elastic modulus of materials [1–3]. The commonly used equations in nanoindentation for calculation of hardness and modulus are as follows:

$$H = \frac{P}{A_c} \tag{1}$$

$$\frac{1-\upsilon^2}{E} = \frac{1}{E_c^*} - \frac{1-\nu_i^2}{E_i} \tag{2}$$

$$E_c^* = \frac{S}{2}\sqrt{\frac{\pi}{A_c}} \tag{3}$$

H being the hardness and E the Young modulus of the material. In Eqs. (1)–(3), P is the applied load, E_c^* is the reduced contact modulus between the tip and the sample, ν and ν_i are the Poisson ratio of the sample and the diamond tip respectively, E_i is the Young modulus of the diamond tip, and A_c is the projected contact area. The Young modulus and the hardness can be calculated by a static method; the properties are determined only at maximum load (Fig. 1), or by a dynamic method, named CSM (continuous stiffness measurement), the properties being measured as a function of the indentation depth, which is not possible with the static method [4]. In Eqs. (1) and (3), all parameters are known or measured by indentation testing, except A_c, the projected contact area. The projected contact area is linked to the contact depth h_c by the tip geometry, for a perfect pyramidal indenter:

$$A_c = \pi \tan^2\theta h_c^2 \tag{4}$$

where θ is the equivalent semi-angle at the apex of the tip. For depths smaller than a few hundred nanometers, the projected contact area can be affected by tip blunting effects. To take into account the non-perfect geometry of the tip, some models have been previously formulated. Oliver and Pharr developed a complex tip area function, using several constants to take blunting of the tip into account [3]. Because of the complex procedure needed to obtain the coefficients, less strenuous models have been developed. For example, Loubet et al. proposed to take into account tip defects by adding a small height to the displacement signal [5]. Other authors have proposed to fit the square root of the projected contact as a function of h_c using linear coefficients, the properties being easier to obtain experimentally for depths higher than 200 nm [6,7]. For smaller depths, other models using power-law or exponential functions have been used [8,9]. Of particular interest, Chicot et al. proposed an area function using a linear and exponential term to account for the tip defect, which can be accurately determined using SEM imaging [10]. The relation between the contact depth h_c and the indentation depth h (measured by indentation technique) is not trivial because the eventual pile-up or sink-in phenomenon that can occur during indentation cannot be determined only with tip displacement measurements. Some models have been developed in order to take into account this phenomenon. For instance, the most commonly used method to calculate h_c is the Oliver and Pharr model, which determines the contact depth with the following equation [3,11]:

$$h_c = h - \varepsilon\frac{P}{S} \tag{5}$$

where $\varepsilon = 0.75$ for a pyramidal indenter. This method can precisely model the sink-in between the sample and the tip, but does not take into account the pile-up, simply because, in Eq. (5), h_c cannot be greater than h. Bolshakov et al. show that the underestimation of the projected contact area can reach up to 60%, for the indented material [11,12], especially if the strain-hardening exponent is very low. Another model proposed by Loubet et al. can be used to calculate the contact depth [5,13]:

$$h_c = \alpha\left(h - \frac{P}{S} + h_0\right) \tag{6}$$

where h_0 is the height used to take into account the tip defect and α is a constant depending on the indenter geometry ($\alpha = 1.2$ for a Berkovich tip [5,13]). Given that α is greater than 1, this model can take into account the pile-up, or sink-in phenomena. Loubet et al. show that this model can estimate precisely the projected contact area for a large range of materials, except for materials with high strain-hardening exponent [5].

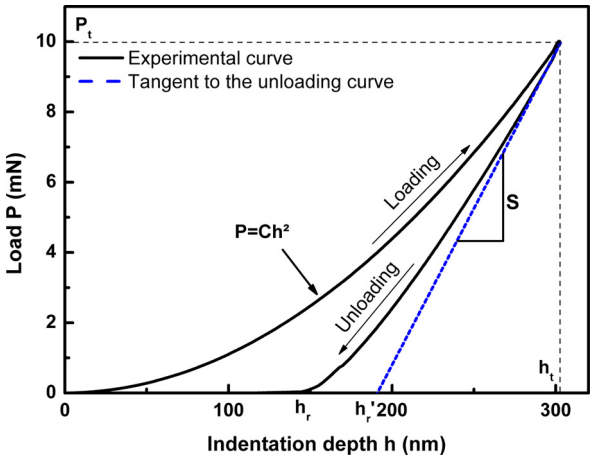

Fig. 1. (Color online.) Loading/unloading curve obtained on an elastoplastic sample. During the loading, the load P is proportional to h^2 through C [3].

One can cite another model based on the calculation of the indentation work [14,15]. It consists in determining the area below the loading–unloading curve, and this area permits the calculation of work performed during indentation. The projected contact area calculated with this method is very close to the value calculated with the Oliver and Pharr model, but, as shown by Cabbibo et al., A_c is not precisely determined for indentation on samples showing a pile-up phenomenon [16]. To quantify pile-up or sink-in, postmortem methods can be used. It consists of calculating the projected contact area after the indentation test. Mc Elaney et al. proposed to calculate A_c after test with SEM images by calculating the ratio between the true area measured and the triangular area of the tip [17]. One can cite also different methods to calculate the pile-up or sink-in, by measuring the lobes of the posttest prints [16]. Measurements of A_c by AFM or scanning probe microscopy using indenter tips can also be performed [18,19]. The projected contact area can be calculated precisely with the post-mortem methods, especially if the material exhibits a purely plastic behavior.

In this paper, a new direct method to determine the projected contact area is proposed. It is independent of any parameter; consequently, it can consider the pile-up or sink-in phenomenon and the strain hardening of the material, which is not possible with the actual direct methods used. It consists in taking advantage of two published and well-known direct methods, used normally for the calculation of the representative indentation stress and strain. They require using two tetrahedral tips with a different semi-angle. In the first part of the paper, the method to measure the projected contact area is presented. It is followed by the description of the experimental tests and the tested samples. The last part will present the results and detail the limits of the technique.

2. Theory

In the last twenty years, many direct methods have been developed to extract the stress–strain curve from nanoindentation results. Some of them are based on the pioneering work of Tabor which shows that the ratio between the hardness and the representative stress is approximately 3 for metallic materials [1]. Other models were developed in order to determine the representative stress and strain for a wide range of materials [20–27]. Among all these models, two will be used for the projected contact area calculation. The first model was developed by Dao et al. [22]. Combining finite-elements simulations and nanoindentation experiments, they developed a reverse analysis of sharp indentation on materials. Dao et al. developed a dimensionless function permitting to calculate the representative stress:

$$\Pi_1 = \frac{C}{\sigma_r} = D_3\left[\ln\left(\frac{E_c^*}{\sigma_r}\right)\right]^3 + D_2\left[\ln\left(\frac{E_c^*}{\sigma_r}\right)\right]^2 + D_1\ln\left(\frac{E_c^*}{\sigma_r}\right) + D_0 \tag{7}$$

where σ_r is the representative stress and D_i are coefficients dependent on the tip geometry and given in Table 1. The reduced contact modulus E_c^* and the loading indentation curvature C (see Fig. 1) are measured from the indentation experiment in order to calculate the representative stress. Using finite-elements simulation and experiments on different aluminum alloys, the dimensionless function developed is independent of the strain-hardening exponent for a representative strain equal to 0.033, which means that the model can calculate properties independently of the strain-hardening exponent. Dao et al. developed this model for Berkovich indentations. The method was extended by Bucaille et al. and Chollacoop et al. [21,24] for other indenter geometries in order to obtain more points in the stress–strain curve (see Table 1). Like Dao et al., they determined a representative strain where the dimensionless function does not depend on the strain-hardening exponent. With the model of Dao et al. extended by Bucaille et al. and Chollacoop et al., accurate properties for the tested materials were determined. The model is limited by the C measurement, performed by a polynomial fit, which can be more difficult for indentation with very sharp indenters. This difficulty in the calculation of C is due to the friction

Table 1
Dao model coefficients as a function of the indenter geometry [21,22,24]. β is the angle between the tip and the sample surface.

β	ε_r	D_3	D_2	D_1	D_0
10°	0.017	−2.913	44.023	−122.771	119.991
19.7°	0.033	−1.131	13.635	−30.594	29.267
30°	0.0537	0.06463	−2.2102	21.589	−28.5741
40°	0.082	0.02937	−0.9324	8.4034	−7.532
47.7°	0.126	0.02842	−0.648	4.9036	−3.806

Table 2
Kermouche model coefficients as a function of the indenter's geometry [28].

β	ζ_1	ζ_2	ζ_3
10°	0.66	0.2	0.22
19.7°	0.66	0.216	0.24
30°	0.66	0.23	0.255
40°	0.66	0.25	0.28
47.7°	0.66	0.26	0.29

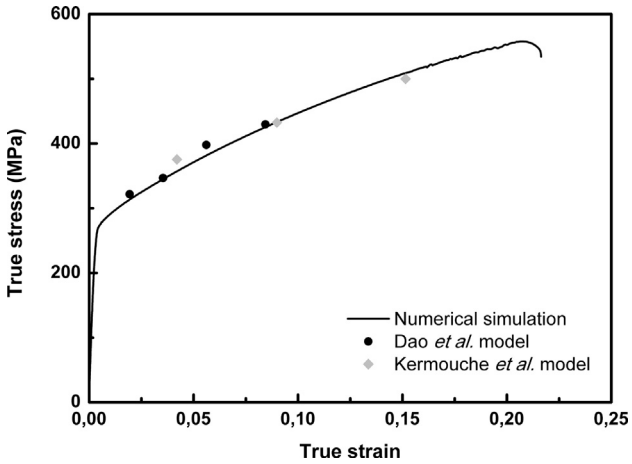

Fig. 2. Stress–strain curve obtained using the Dao et al. and the Kermouche et al. models with different indenter tip geometries. Dao et al. and Kermouche et al. points were determined from numerical simulation of an indentation on a Cu–Zn sample. For a representative strain equal to 0.082, the representative stresses obtained with the two models are approximately equal.

between the tip and the sample, which can affect the loading curve. The Indentation Size effect, which means that hardness is not constant for small penetration depths, is the second limit of the C calculation, because it implies that C is not constant with penetration [24]. Another important point is that the projected contact area is needed in order to calculate the reduced contact modulus E_c^*.

The second model used to calculate the projected contact area was developed by Kermouche et al. It was validated by finite-elements simulations and experiments on metallic materials and polymers [28,29]. The model needs prior knowledge of the hardness H and the Young modulus E of the material (measured by an indentation test) in order to calculate the representative stress and strain:

$$\sigma_r = \frac{\zeta_3 \tan(\beta) H}{\zeta_1 \tan(\beta) - (1-\zeta_2)\frac{H}{E}} \tag{8a}$$

$$\varepsilon_r = (1-\zeta_2)\frac{\sigma_r}{E} + \zeta_3 \tan(\beta) \tag{8b}$$

where β is the angle between the tip face and the sample, and ζ_i are coefficients determined by Kermouche et al., dependent on the tip's geometry (see Table 2). The values of H and E are determined by an indentation test, which means that the determination of the projected contact area is needed.

Like in the Dao et al. model, Kermouche et al. determined the representative stress and strain with different indenter geometries. An example is shown in Fig. 2, presenting the stress–strain curve determined with the model using a finite-element simulation of the indentation on a Cu–Zn sample.

The points obtained with these two models follow precisely the stress–strain behavior of the Cu–Zn alloy used in the numerical simulation. It can be noticed that representative strains computed with tip angles of 20° and 40°, respectively,

for the models of Dao et al., on the one hand, and of Kermouche et al., on the other hand, are very close. Hence, a new equation can be added to the set of equations already available:

$$\sigma_{r,K} = \sigma_{r,D} \tag{9}$$

where K corresponds to the Kermouche model and D to the Dao model. If we insert Eq. (8a) into Eq. (7), one can obtain the following equation:

$$C = \sigma_{r,K}\left(D_3\left[\ln\left(\frac{E_c^*}{\sigma_{r,K}}\right)\right]^3 + D_2\left[\ln\left(\frac{E_c^*}{\sigma_{r,K}}\right)\right]^2 + D_1\ln\left(\frac{E_c^*}{\sigma_{r,K}}\right) + D_0\right) \tag{10a}$$

$$\sigma_{r,K} = \frac{\zeta_3\tan(\beta)H}{\zeta_1\tan(\beta) - (1-\zeta_2)\frac{H}{E}} \tag{10b}$$

In Eqs. (10a) and (10b), the ζ_i and D_i coefficients are known and presented in Tables 1 and 2, β is given by the tip geometry, and C is determined directly by fitting the loading curve. Only the hardness, the reduced contact modulus and the Young modulus are not known. The objective is to calculate the projected contact area with the combination of the models. In other words, the equation has to contain only one unknown parameter, which is the projected contact area. The reduced contact modulus E_c^* is a function of the projected contact area through Eq. (3). The Young modulus depends on the reduced contact modulus through Eq. (2), so E depends only on the projected contact area. Finally, the hardness is also dependent on the projected contact area through Eq. (1). Consequently, Dao's and Kermouche's models can be written as follows:

$$C = \sigma_{r,K}\left(D_3\left[\ln\left(\frac{E_c^*}{\sigma_{r,K}}\right)\right]^3 + D_2\left[\ln\left(\frac{E_c^*}{\sigma_{r,K}}\right)\right]^2 + D_1\ln\left(\frac{E_c^*}{\sigma_{r,K}}\right) + D_0\right) \tag{11a}$$

$$\sigma_{r,K} = \frac{\zeta_3\tan(\beta)H}{\zeta_1\tan(\beta) - (1-\zeta_2)\frac{H}{E}} \tag{11b}$$

$$E = \frac{1-\upsilon^2}{(\frac{1}{E_c} - \frac{1-\nu_i^2}{E_i})} \tag{11c}$$

$$E_c = \frac{S}{2}\sqrt{\frac{\pi}{A_c}} \tag{11d}$$

$$H = \frac{P}{A_c} \tag{11e}$$

Inserting Eqs. (11c)–(11e) into Eqs. (11a) and (11b), the DK (Dao and Kermouche) model is only dependent on the projected contact area, given that E_i, ν, ν_i, D_i and ζ_i, are known and S (stiffness at maximum load), P (maximum load), and C are measured directly from indentation testing. Using Eq. (1), the material hardness can also be calculated, then the Young modulus with Eqs. (2) and (3). An important point has to be considered in Eqs. (11). In order to satisfy the equality in Eq. (9), the Dao parameter C has to be determined by an indentation using a tip with $\beta = 40°$ (β being the angle between the tip and the sample's surface), and the parameters S and P, necessary for the Kermouche et al. model, have to be determined with an indentation with a Berkovich tip.

3. Experimental application

3.1. Samples

Three smooth samples were tested in the experiment: glass, PMMA, and 100C6 steel. These materials were chosen in order to apply the method for different types of materials: the glass sample is supposed to be amorphous and brittle, PMMA is a viscoelastic and amorphous material and 100C6 steel exhibits an elastoplastic behavior and a crystalline structure. Samples were glued with cyanoacrylate on an aluminum plot.

3.2. Nanoindenter

A nanoindenter XP® (Agilent Technologies) was used for the experiments. The load and displacement resolutions are 10 nN and 0.5 nm, respectively. A more detailed description of the apparatus is presented in [30]. A Berkovich diamond tip (tip defect height $h_0 = 15$ nm approximately, measured with the Loubet method on a fused silica sample [5]) and a diamond tip with $\beta = 40°$ (tip defect negligible) were used. For each sample, loading and unloading were performed at constant strain rate, with $\dot{P}/P = 0.03\ s^{-1}$ [31], except for the PMMA sample, where $\dot{P}/P = 0.03\ s^{-1}$ for Berkovich indentation and $\dot{P}/P = 0.07\ s^{-1}$ for indentations with the sharpest tip [32]. For indentations with the sharpest tip, the CSM method was not used in order to avoid oscillation effects in the C calculation [33]. The CSM method was used for indentations with Berkovich tip in order to measure the contact stiffness necessary in the Kermouche model. The oscillation frequency and the amplitude were 32 Hz and 1 nm respectively. Ten indents were performed on each sample with the two indenter tips.

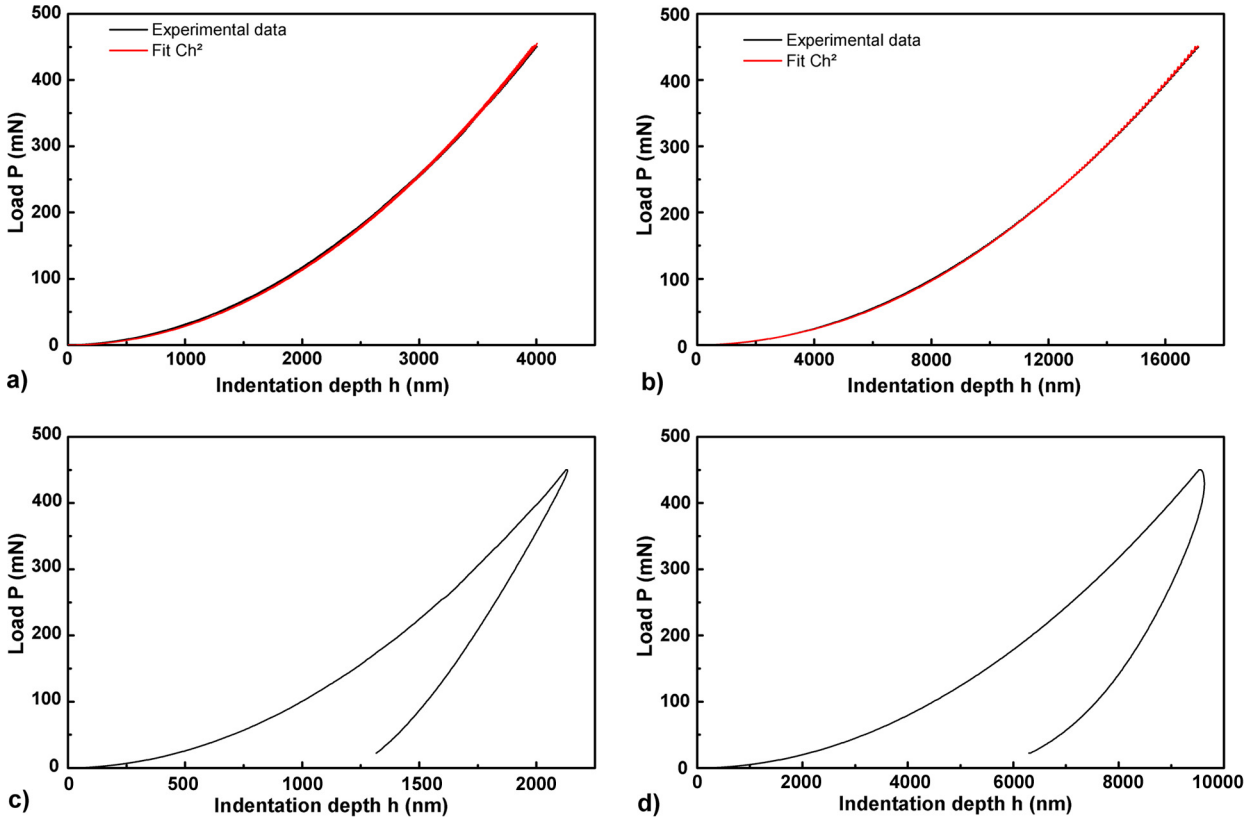

Fig. 3. (Color online.) Load–indentation depth for glass (a and c) and PMMA (b and d) samples. a, b) Load–indentation depth measured with a tip where $\beta = 40°$ with a polynomial fit to obtain C. c, d) Load–indentation depth curves measured with a Berkovich tip to obtain P and S.

Table 3
Parameters used in the models to calculate the projected contact area and the material's properties. Comparison with values obtained by the Oliver and Pharr model and the Loubet et al. model.

Data	PMMA	Glass	100C6 steel
P (mN)	450	450	450
S (N/m)	271 341	669 359	1 618 025
C (N/m^2)	1.53E+09	2.86E+10	4.39E+10
E^* Dao and Kermouche (GPa)	5.94	67.95	223.96
E^* Loubet (GPa)	5.10	72.35	213.01
E^* Oliver and Pharr (GPa)	5.78	73.70	249.70
H Dao and Kermouche (GPa)	0.273	5.27	7.988
H Loubet (GPa)	0.21	5.77	7.32
H Oliver and Pharr (GPa)	0.27	6.76	9.53
A_c Dao and Kermouche (µm^2)	1668.5	85.39	56.33
Ac Loubet (µm^2)	2193.07	75.35	63.25
A_c Oliver and Pharr (µm^2)	1687.94	65.04	48.34
Poisson ratio ν	0.30	0.30	0.30

4. Results

In Fig. 3 are presented the load–displacement curves obtained on a glass sample and a PMMA sample with the two indenter geometries. In Figs. 3a and b, showing the indentation loading curves on glass and PMMA with the sharpest tip, a polynomial fit was performed in order to calculate the C coefficient. The fit curve follows exactly the experimental curve, which means that the C coefficient can be calculated very precisely. The mean value of C determined from 10 indentations for glass and PMMA samples is presented in Table 3. The C value obtained from glass sample is higher than the value obtained on the PMMA sample because the glass sample is harder than the PMMA sample. In Figs. 3c and d are presented the loading–unloading curves obtained on glass and PMMA samples, for an indentation with the Berkovich tip. For the PMMA sample, one can note the 'nose' at the beginning of the unloading, which prevents any calculation of the unloading stiffness by the static method. The dynamic stiffness determined with the CSM method at maximum load for the two samples is given in Table 3. In this table are also presented the elastic modulus, the hardness and the projected contact area

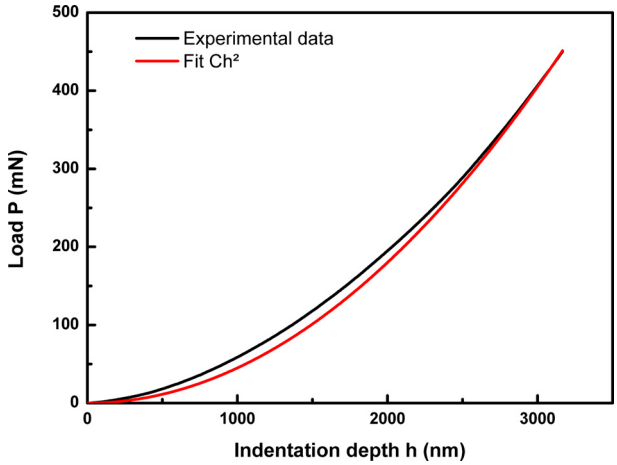

Fig. 4. (Color online.) Load–indentation depth curve for a 100C6 sample measured with a tip where $\beta = 40°$, with a polynomial fit to obtain C.

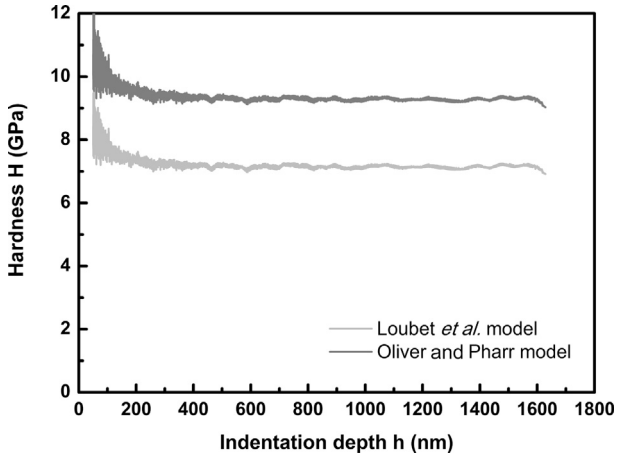

Fig. 5. 100C6 steel hardness measured with a Berkovich tip as a function of the indentation depth.

determined by the DK model and by the Loubet et al. and the Oliver and Pharr models. For a glass sample, A_c obtained with the DK model is closer to A_c obtained with the Loubet et al. model (12% error) in comparison to the value obtained with the Oliver and Pharr model (24% error). It is known that the Oliver and Pharr method underestimates the projected contact area for materials that do not exhibit strain hardening mechanism, like the glass sample [19,34]. On the PMMA sample, the value of A_c obtained with the DK method is very close to that obtained with the Oliver and Pharr method (1% error), whereas that obtained by the Loubet et al. model is overestimated by 30%. It is known that PMMA exhibits sink-in during indentation and the Oliver and Pharr model models precisely the sink-in behavior, which explains this small difference [11]. This method permits to show that the Loubet et al. model and the Oliver and Pharr model calculate the projected contact area with enough accuracy only for a certain range of materials. In the following paragraph, the limits of the technique are shown and discussed.

5. Limits of the method

In Fig. 4 is presented the loading curve obtained on a 100C6 sample indented by the sharpest tip. The polynomial fit is plotted to calculate C. The parabolic fit does not provide a satisfying result when it is applied on the entire curve, leading to a bad estimation of load curvature C. Bucaille et al. explain that the friction coefficient is more important for tips having high β values and that can affect the load–displacement curve. They also mentioned that the size effect can occur for metallic materials, which means that the hardness increases as the indentation depth decreases [24]. For the last point, in order to detect any size effect during indentation of the 100C6 sample, the hardness was plotted as a function of the indentation depth, the values being calculated with the Oliver and Pharr model and with the Loubet et al. model (Fig. 5). With the two methods, the hardness decreases for indentation depths between 50 and 300 nm. At this range of depth, tip defects can affect property measurement; however, the reduced elastic modulus measured on this sample (not shown in this paper) was constant at this range of depth, indicating that the hardness increase at small depths is predominately

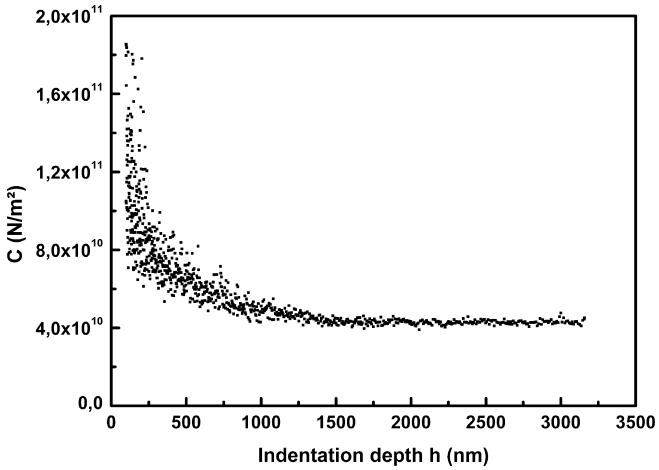

Fig. 6. Evolution of C calculated locally as a function of the indentation depth for a 100C6 steel sample.

due to an ISE. To confirm the ISE, the C coefficient was calculated locally on the loading curve and plotted in Fig. 6. One can observe that C is constant for indentation depths higher than 1500 nm, showing that we can consider the material to be homogeneous only for this range of depths. For lower depths, the C values are increasing as the indentation depth decreases. This figure confirms the presence of ISE, leading to difficulties in C value calculation. In order to calculate C precisely, we determined the average value of C for the depth range where the size effect is negligible, i.e. at depths higher than 1500 nm. In Table 3 are shown the properties and the projected contact area determined with the Dao and Kermouche model, C being calculated using the mean local value for depths higher than 1500 nm. The values obtained with the DK model are closer to the values obtained with the Loubet et al. model (12%) than to the ones calculated using the Oliver and Pharr model (14%). Because the literature values of Young's modulus are very close to that obtained with the Dao and Kermouche model, we can consider that the friction coefficient has small influence on the loading curve in our case.

6. Conclusions

A new method to estimate the true projected contact area by indentation testing has been presented. It is based on the combination of the Dao et al. model and the Kermouche et al. model, these models used classically to calculate the representative stress and strain from indentation parameters. More importantly, the Dao et al. model requires the reduced contact modulus and the loading curvature value extracted from an indentation test, and the Kermouche et al. model requires the Young modulus and the hardness of the sample. For a representative strain equal to 0.082, the representative stress determined by the two models is approximately the same. Consequently, the two models can be combined, which leads to an equation that is dependent only on the projected contact area. Using the parameters measured by nanoindentation, the projected contact area can be calculated directly, without using the classical models of Oliver and Pharr, or Loubet et al. It requires determining the loading curvature C, the load applied and the contact stiffness S. In order to extract these parameters, indentations with a Berkovich tip (to extract S and P) and a tip with $\beta = 40^\circ$ (to extract C) on the same sample have to be performed. The method was first applied on a glass sample and a PMMA sample. The calculation of C, necessary for the model, is easily feasible by a simple polynomial fit. However, for a 100C6 steel sample, the polynomial fit was more difficult to perform on the loading curve. We show that this phenomenon is mainly caused by the Indentation Size Effect, which predicts that hardness increases for small penetration depths, leading to a difficult C estimation, because the approach proposed here has been developed for homogeneous materials. To bypass this problem, a local calculation of C can be performed. We show that for large indentation depths, the ISE becomes negligible, C being constant with depth. Using the C value obtained locally, the projected contact area can be calculated with enough accuracy, the values of modulus and hardness obtained being close to the literature values.

References

[1] D. Tabor, The hardness of solids, Rev. Phys. Technol. 1 (1970) 145–179.
[2] S.I. Bulychev, V.P. Alekhin, M.K. Shorshorov, A.P. Ternovskii, G.D. Shnyrev, Determining Young modulus from the indenter penetration diagram, Ind. Lab. USSR Engl. Transl. Zavod. Lab. 41 (1975) 1409–1412.
[3] W.C. Oliver, G.M. Pharr, An improved technique for determining hardness and elastic-modulus using load and displacement sensing indentation experiments, J. Mater. Res. 7 (1992) 1564–1583.
[4] S.A.S. Asif, K.J. Wahl, R.J. Colton, Nanoindentation and contact stiffness measurement using force modulation with a capacitive load–displacement transducer, Rev. Sci. Instrum. 70 (1999) 2408–2413.
[5] J.-L. Loubet, M. Bauer, A. Tonck, S. Bec, B. Gauthier-Manuel, Nano-indentation with a surface force apparatus, NATO Adv. Study Inst. Ser. E (1993) 429–447.

[6] J. Thurn, R.F. Cook, Simplified area function for sharp indenter tips in depth-sensing indentation, J. Mater. Res. 17 (2002) 1143–1146.
[7] M. Troyon, L. Huang, Comparison of different analysis methods in nanoindentation and influence on the correction factor for contact area, Surf. Coat. Technol. 201 (2006) 1613–1619.
[8] H. Bei, E.P. George, J.L. Hay, G.M. Pharr, Influence of indenter tip geometry on elastic deformation during nanoindentation, Phys. Rev. Lett. 95 (2005).
[9] J.M. Antunes, A. Cavaleiro, L.F. Menezes, M.I. Simões, J.V. Fernandes, Ultra-microhardness testing procedure with Vickers indenter, Surf. Coat. Technol. 149 (2002) 27–35.
[10] D. Chicot, M. Yetna N'Jock, E.S. Puchi-Cabrera, A. Iost, M.H. Staia, G. Louis, et al., A contact area function for Berkovich nanoindentation: application to hardness determination of a TiHfCN thin film, Thin Solid Films 558 (2014) 259–266.
[11] W.C. Oliver, G.M. Pharr, Measurement of hardness and elastic modulus by instrumented indentation: advances in understanding and refinements to methodology, J. Mater. Res. 19 (2004) 3–20.
[12] A. Bolshakov, G.M. Pharr, Influences of pileup on the measurement of mechanical properties by load and depth sensing indentation techniques, J. Mater. Res. 13 (1998) 1049–1058.
[13] G. Hochstetter, A. Jimenez, J.-L. Loubet, Strain-rate effects on hardness of glassy polymers in the nanoscale range. Comparison between quasi-static and continuous stiffness measurements, J. Macromol. Sci. Part B Phys. 38 (1999) 681.
[14] J.R. Tuck, A.M. Korsunsky, S.J. Bull, R.I. Davidson, On the application of the work-of-indentation approach to depth-sensing indentation experiments in coated systems, Surf. Coat. Technol. 137 (2001) 217–224.
[15] D. Beegan, S. Chowdhury, M.T. Laugier, Work of indentation methods for determining copper film hardness, Surf. Coat. Technol. 192 (2005) 57–63.
[16] M. Cabibbo, P. Ricci, True hardness evaluation of bulk metallic materials in the presence of pile up: analytical and enhanced lobes method approaches, Metall. Mater. Trans. A 44 (2013) 531–543.
[17] K.W. McElhaney, J.J. Vlassak, W.D. Nix, Determination of indenter tip geometry and indentation contact area for depth-sensing indentation experiments, J. Mater. Res. 13 (1998) 1300–1306.
[18] D. Beegan, S. Chowdhury, M.T. Laugier, The nanoindentation behaviour of hard and soft films on silicon substrates, Thin Solid Films 466 (2004) 167–174.
[19] L. Charleux, V. Keryvin, M. Nivard, J.-P. Guin, J.-C. Sanglebœuf, Y. Yokoyama, A method for measuring the contact area in instrumented indentation testing by tip scanning probe microscopy imaging, Acta Mater. 70 (2014) 249–258.
[20] K.L. Johnson, The correlation of indentation experiments, J. Mech. Phys. Solids 18 (1970) 115–126.
[21] N. Chollacoop, M. Dao, S. Suresh, Depth-sensing instrumented indentation with dual sharp indenters, Acta Mater. 51 (2003) 3713–3729.
[22] M. Dao, N. Chollacoop, K.J. Van Vliet, T.A. Venkatesh, S. Suresh, Computational modeling of the forward and reverse problems in instrumented sharp indentation, Acta Mater. 49 (2001) 3899–3918.
[23] J.-L. Bucaille, E. Felder, G. Hochstetter, Identification of the viscoplastic behavior of a polycarbonate based on experiments and numerical modeling of the nano-indentation test, J. Mater. Sci. 37 (2002) 3999–4011.
[24] J.-L. Bucaille, S. Stauss, E. Felder, J. Michler, Determination of plastic properties of metals by instrumented indentation using different sharp indenters, Acta Mater. 51 (2003) 1663–1678.
[25] Y.-T. Cheng, C.-M. Cheng, Scaling, dimensional analysis, and indentation measurements, Mater. Sci. Eng. R Rep. 44 (2004) 91–149.
[26] A. Constantinescu, N. Tardieu, On the identification of elastoviscoplastic constitutive laws from indentation tests, Inverse Probl. Eng. 9 (2001) 19–44.
[27] X. Hernot, C. Moussa, O. Bartier, Study of the concept of representative strain and constraint factor introduced by Vickers indentation, Mech. Mater. 68 (2014) 1–14.
[28] G. Kermouche, J.-L. Loubet, J.-M. Bergheau, An approximate solution to the problem of cone or wedge indentation of elastoplastic solids, C. R. Mecanique 333 (2005) 389–395.
[29] G. Kermouche, J.-L. Loubet, J.-M. Bergheau, Extraction of stress–strain curves of elastic–viscoplastic solids using conical/pyramidal indentation testing with application to polymers, Mech. Mater. 40 (2008) 271–283.
[30] G. Guillonneau, G. Kermouche, S. Bec, J.-L. Loubet, Extraction of mechanical properties with second harmonic detection for dynamic nanoindentation testing, Exp. Mech. 52 (2012) 933–944.
[31] B.N. Lucas, W.C. Oliver, G.M. Pharr, J.-L. Loubet, Time dependent deformation during indentation testing, in: Proc. 1996 MRS Spring Meet, April 8 1996 – April 12 1996, San Francisco, CA, USA, 1996, pp. 233–238.
[32] G. Kermouche, J.-L. Loubet, J.-M. Bergheau, Cone indentation of time-dependent materials: the effects of the indentation strain rate, Mech. Mater. 39 (2007) 24–38.
[33] G.M. Pharr, J.H. Strader, W.C. Oliver, Critical issues in making small-depth mechanical property measurements by nanoindentation with continuous stiffness measurement, J. Mater. Res. 24 (2009) 653–666.
[34] M.Y. N'jock, D. Chicot, J.M. Ndjaka, J. Lesage, X. Decoopman, F. Roudet, et al., A criterion to identify sinking-in and piling-up in indentation of materials, Int. J. Mech. Sci. 90 (2015) 145–150.